



Experimental Study of FRP-Steel-UHPC Composite Tube Confined Seawater Sea-Sand Concrete Columns Under Axial Compression

Lan Zeng¹, Xuqi Liang¹, Zurui Liu¹, Hong Yuan^{2*}

¹Key Laboratory of Green toughening and safety prevention and control of offshore structures, School of Mechanics and Construction Engineering, Jinan University, Guangzhou 510632, P.R. China

²School of Architectural Engineering, Guangzhou Institute of Science and Technology, Guangzhou, Guangdong 510540, P.R. China

*Corresponding author's e-mail: tyuanhong@jnu.edu.cn

Abstract. To address the prevalent issues of low lateral resistance and ductility in corrosion-resistant FRP-confined members, as well as weak FRP-concrete interfacial bonding, this paper proposes a novel marine engineering structural component: FRP-steel-ultra-high performance concrete (UHPC) composite tube (FRP-steel-UHPC composite tube) confined seawater and sea-sand concrete (SSC) columns (FSU-SSCs). To investigate their axial compression performance, axial compression tests were conducted on five FSU-SSCs. The test results indicate that FRP-steel-UHPC composite tubes significantly enhances the axial compressive behavior of the confined SSC compared to FRP-steel or steel-UHPC composite tubes. Increasing FRP layers, steel tube thickness, and UHPC thickness improves load-bearing capacity and deformation of the composite columns, with multiple GFRP layers showing non-linear cumulative effects. The load-bearing capacity and the ultimate strain of FSU-SSC with a 30-mm UHPC shell respectively increased by 11.5% and 25.56% compared to that with a 20-mm UHPC shell.

Keywords: Seawater and sea sand; Ultra-high performance concrete; FRP-steel composite structure; Axial compression characteristics.

1 Introduction

Reinforced concrete structures using ordinary concrete represent one of the most significant types of construction projects in contemporary engineering. Nevertheless, the increasing scarcity of river sand and freshwater resources, coupled with extraction and purification challenges, has led to substantial adverse impacts on inland ecosystems [1]. Utilizing the relatively abundant seawater and sea sand resources in marine engineering could mitigate the reliance on inland resources, reduce ecological damage, lower the

transportation costs of raw materials, and enhance the economic efficiency of construction endeavors [2, 3]. However, chloride ions in sea sand corrode steel reinforcement, limiting its use. [3].

With the advancement of new materials, the corrosion resistance of fiber-reinforced polymer (FRP) has shown significant potential for use in offshore structures [4, 5]. In seawater sea-sand concrete (SSC) columns confined by FRP, the FRP tubes not only provide corrosion resistance but also offer confinement, enhancing mechanical performance and serving as prefabricated molds. However, due to the typically annular fiber orientation of FRP tubes and the material brittleness, the FRP-steel composite tube effectively addresses the issue of low lateral resistance and stability in single FRP-confined concrete [6, 7]. Nevertheless, when FRP is employed as an isolation layer between steel and SSC, challenges arise due to the weak interfacial bonding between FRP and concrete [8, 9]. This inadequate bonding compromises the synergistic interaction of the components, ultimately affecting the structural performance. Consequently, the separation strategy between steel and SSC requires careful reconsideration.

Ultra-high performance concrete (UHPC) exhibits exceptional load-bearing capacity and superior durability, enabling it to withstand substantial structural loads and prevent chloride ion penetration [10]. As a cement-based material, UHPC demonstrates excellent interfacial bonding properties with steel tubes as concrete [11], making it particularly advantageous as an interlayer between steel tubes and SSC. While UHPC shells have been successfully implemented in novel offshore composite structures, their potential for interface performance enhancement remains relatively unexplored in such applications [12, 13]. To address this limitation, this study proposes an innovative structural component specifically designed for marine engineering: the FRP-steel-UHPC composite tube confined SSC column (FSU-SSC), as illustrated in Figure 1.

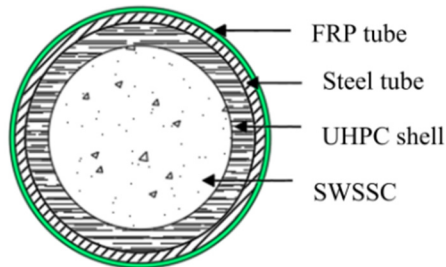


Fig. 1. Cross-section of FSU-SSC.

2 Experimental Program

2.1 Test Design

A total of seven specimens were designed, including five FSU-SSCs, along with one FRP-steel composite tube confined SSC column and one steel-UHPC composite tube confined SSC column as controls. The specimens were short columns with a height of 490 mm and a diameter of 245 mm. The experimental parameters included: the number

of FRP layers (6 and 9), the thickness of the steel tube (4 mm and 6 mm), the thickness of the UHPC shell (20 mm and 30 mm), and the loading scheme (monotonic and cyclic). The specimen design is detailed in Table 1.

Table 1. Parameter design of each specimen.

Specimen	FRP fiber type	FRP fiber layer	Steel tube thickness (mm)	UHPC shell thickness (mm)	Loading scheme
M-G6-S4	Glass	6	4	—	Monotonic
M-S4-U20	—	—	4	20	Monotonic
M-G6-S4-U20	Glass	6	4	20	Monotonic
M-G9-S4-U20	Glass	9	4	20	Monotonic
M-G6-S6-U20	Glass	6	6	20	Monotonic
M-G6-S4-U30	Glass	6	4	30	Monotonic
C-G6-S4-U20	Glass	6	4	20	Cyclic

2.2 Material Properties

The SSC was of strength grade C40, with a mix ratio of cement: seawater: fine aggregate: coarse aggregate = 1: 0.49: 1.33: 2.53. The seawater was artificially prepared according to the ASTM D1141-2013 standard. The mix ratio for UHPC was cement: stainless steel fiber: fine sand: silica fume: fly ash: water reducer: adhesive powder = 1: 0.08: 0.735: 0.045: 0.265: 0.0045: 0.01. The axial compressive strengths of SSC and UHPC were 45.13MPa and 125.58MPa, respectively, with calculated elastic moduli of 26.90GPa and 41.49GPa, respectively.

Seamless steel tubes of Q235 grade were utilized. According to the GB/T 228.1-2010 standard, tensile tests were conducted on steel coupons, yielding a yield strength of 265.12MPa, an elastic modulus of 205.63 GPa, a tensile strength of 322.05 MPa, and an elongation of 38%. Following the ASTM D3039 standard, tensile tests on GFRP coupons yielded an average elastic modulus of 90.32 GPa, a tensile strength of 1658.28 MPa, and an ultimate strain of 1.67%.

2.3 Specimen Preparation

The fabrication of test specimens primarily involved as illustrated in Figure 2: a) FRP-steel composite tube manufacturing: Strain gauges were attached to the steel tube, fiber sheets adhered with epoxy resin. b) UHPC shell fabrication: Using the FRP-steel composite tube as the outer mold and a foam cylinder coated with a release agent as the inner mold, UHPC was poured between the molds. After the UHPC had set, the inner foam cylinder was removed. c) SSC casting and curing: The FRP-steel-UHPC composite tube served as the mold, into which SSC was poured and subsequently cured. d) Pre-loading treatment: External FRP strain gauges and displacement meter fixtures were attached.

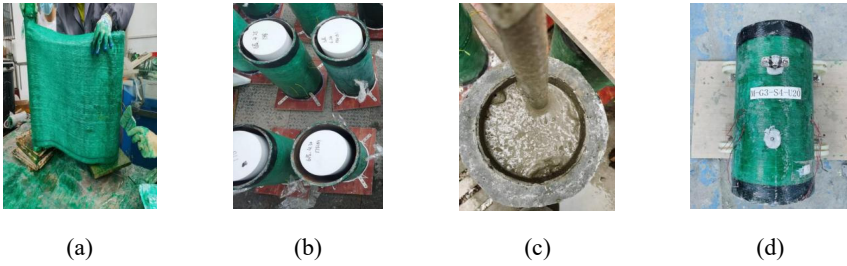
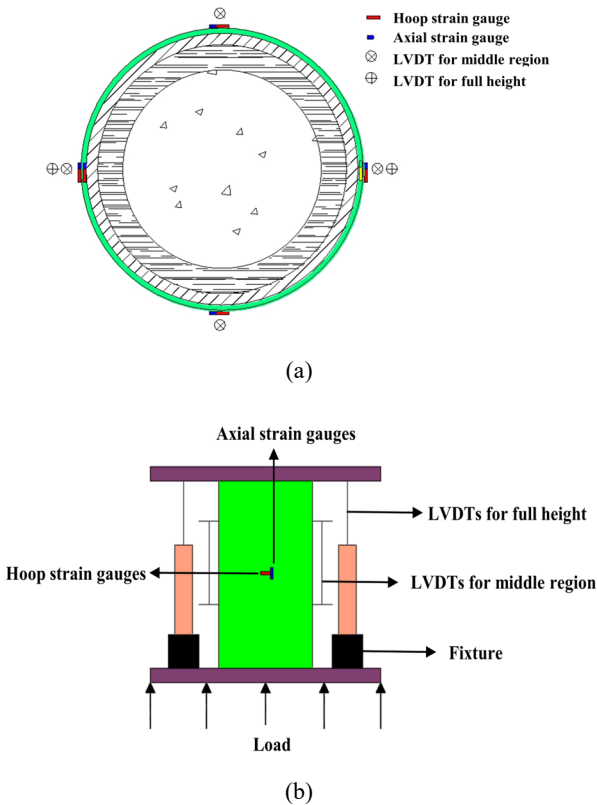
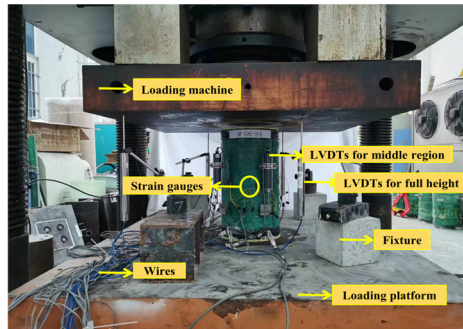


Fig. 2. Specimen preparation procedure: a) FRP-steel composite tube manufacturing; b) UHPC shell fabrication; c) SSC casting and curing; d) Pre-loading treatment.

2.4 Test setup and Measurements

At the mid-height of the specimen, four sets of hoop and axial strain gauges were evenly spaced around the circumference. Additionally, two groups of four linear variable displacement transducers (LVDTs) were evenly distributed around the circumference along the middle and full height of the column. The loading setup and the layout of measurements are illustrated in Figure 3.





(c)

Fig. 3. Arrangement of measurement points and the loading setup: a) Cross-sectional measurement points; b) Side measurement points; c) Loading diagram.

3 Experimental Results and Discussion

3.1 Failure Modes

Figure 4 shows the failure modes for each specimen. During the initial stage of loading, the concrete primarily bore the load, and no significant changes were observed on the surface of the specimen. As the load increased, the steel tube began to exhibit buckling, at which point the surface of the FRP started to whiten, accompanied by a sizzling sound. When the load reached 85% of the peak, major cracks began to appear in the FRP, accompanied by rapid cracking noises. The load continued to increase until it reached the ultimate load, at which point the FRP emitted a loud bang as it fractured, leading to the failure of the specimen.

Specimen M-G6-S4 exhibited a bulging shape at the mid-height, while M-G6-S4-U20 showed a nearly parallel shape along the edges of the entire column. This indicates that the addition of the UHPC shell layer plays a significant role in controlling the expansion deformation of the component, particularly in restraining the expansion of the concrete. Furthermore, the presence of the UHPC shell layer allows the steel tube to undergo more uniform circumferential deformation, which contributes to improving the specimen ductility. Increasing the thickness of each component of the composite tube can reduce the length and width of the main crack regions in the FRP. Cyclic loading increases the degree of fragmentation in the mid-section of the FRP.

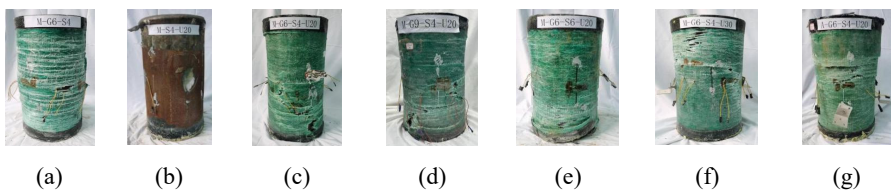


Fig. 4. Failure modes: a) M-G6-S4; b) M-S4-U20; c) M-G6-S4-U20; d) M-G9-S4-U20; e) M-G6-S6-U20; f) M-G6-S4-U30; g) C-G6-S4-U20.

3.2 Key Test Results

The ultimate load N_u , the ultimate axial strain ε_u corresponding to the ultimate load, the residual load N_r , and the hoop strain ε_h at the time of external fiber fracture for each specimen are listed in Table 2. The average ratio of residual load to ultimate load for specimens is 75.7%, indicating high post-peak load-bearing capacity. Increasing the thickness of each component of the FRP-steel-UHPC composite tube enhances the axial compression performance of FSU-SSCs. Specifically, the specimen with 9-layer GFRP shows an increase of 33.79%, 50.26%, and 26.83% in cracking load, ultimate bearing capacity, and hoop strain at FRP fracture, respectively, compared to that with 6-layer GFRP. Increasing the thickness of the steel tube significantly enhances the deformation capacity of the member. The specimen with a 6-mm-thick steel tube exhibits a 53.19% increase in ultimate displacement compared to that with a 4-mm-thick steel tube. The specimen with a 30-mm UHPC shell shows an 11.50% and 25.56% improvement in ultimate bearing capacity and ultimate strain, respectively, compared to that with a 20-mm one.

Table 2. Key test results.

Specimen	N_u (kN)	ε_u	N_r (kN)	N_r / N_u	ε_h
M-G6-S4	5992.9	2.47%	4533.5	0.75	0.11%
M-S4-U20	3847.9	1.10%	2741.1	0.71	—
M-G6-S4-U20	6340.4	2.66%	4861.6	0.76	1.23%
M-G9-S4-U20	8482.8	3.17%	7305.0	0.86	1.56%
M-G6-S6-U20	7549.8	4.08%	5826.0	0.77	1.36%
M-G6-S4-U30	7069.5	3.34%	4899.7	0.69	1.30%

The axial load-displacement curves for each specimen are illustrated in Figure 5. These curves can generally be divided into four stages: In the first elastic stage, as the load increases, the displacement of specimens also increases, and a relatively clear linear relationship between load and displacement is observed. In the second yielding stage, the steel tube begins to yield, and the slope of the load-displacement curve significantly decreases. The confinement effect of the steel tube on the UHPC shell weakens, while the restraining effect of the FRP starts to strengthen. In the third development stage, the member reaches its ultimate bearing capacity, and the buckling and expansion of the steel tube become more pronounced. Since the yielded steel tube can only provide a relatively constant lateral restraining force, the primary restraining role shifts to the external FRP until the FRP fractures. In the fourth descending stage, after reaching the peak ultimate load, the member enters the stable descending phase, demonstrating good ductility. Additionally, for both loading methods, there is a notable consistency and overlap between the load-displacement curve obtained from monotonic axial compression tests and the envelope curve derived from cyclic axial compression tests.

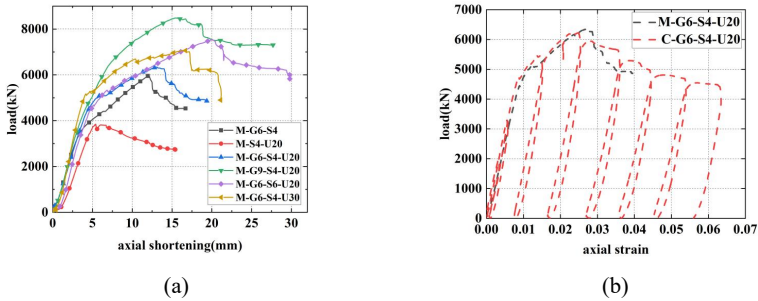


Fig. 5. load-axial shortening curves of each specimen: a) monotonic loading; b) cyclic loading.

3.3 Effect of Different Test Parameters

As shown in Figure 6a, the initial elastic development stages of the load-axial strain curves for specimens with different FRP layers almost overlap, indicating that the external FRP has a minimal constraining effect on the specimens at this stage. However, increasing the number of external FRP layers extends the elastic segment of the curve and delays the yield segment, suggesting a significant slowdown in the yielding of the steel tube. The increase in external FRP layers also prolongs the ascending segment of the curve and increases its slope, ultimately achieving higher ultimate axial strain and ultimate load. Additionally, it reduces the curvature of the descending segment, demonstrating greater residual load capacity and ductility. Even after experiencing large axial strains, the component can still withstand relatively high loads, showcasing excellent post-failure load-bearing capacity. Under the same load, the hoop strain of the component decreases as the number of GFRP layers increases. This indicates that GFRP can effectively restrain the lateral expansion of the steel tube during buckling, slowing down the deformation rate.

In Figure 6b, it can be observed that the linear segments and yield points of the load-displacement curves for specimens with different steel tube thicknesses essentially coincide. However, specimens with thicker steel tubes exhibit a longer third segment in the load-displacement curve, demonstrating higher ultimate load capacity and residual load. Nevertheless, the slopes of the ascending and descending segments in the third and fourth stages are nearly identical. Since the steel tube can approximately maintain a circular shape after yielding, this geometric stability is crucial for supporting the internal concrete structure. As the thickness of the steel tube increases, its constraining effect on the concrete during the post-failure stage becomes more pronounced, thereby enhancing the overall residual load capacity of the composite column.

In Figure 6c, a larger UHPC shell thickness can increase the slope of the linear segment of the load-displacement curve, reflected in higher initial stiffness and greater yield load. It also extends the rising segment of the third stage of the curve, demonstrating higher ultimate bearing capacity, though it has a smaller impact on the slope of this segment. A thicker UHPC shell plays a positive role in restricting circumferential expansion and enhancing the overall structural integrity of the member.

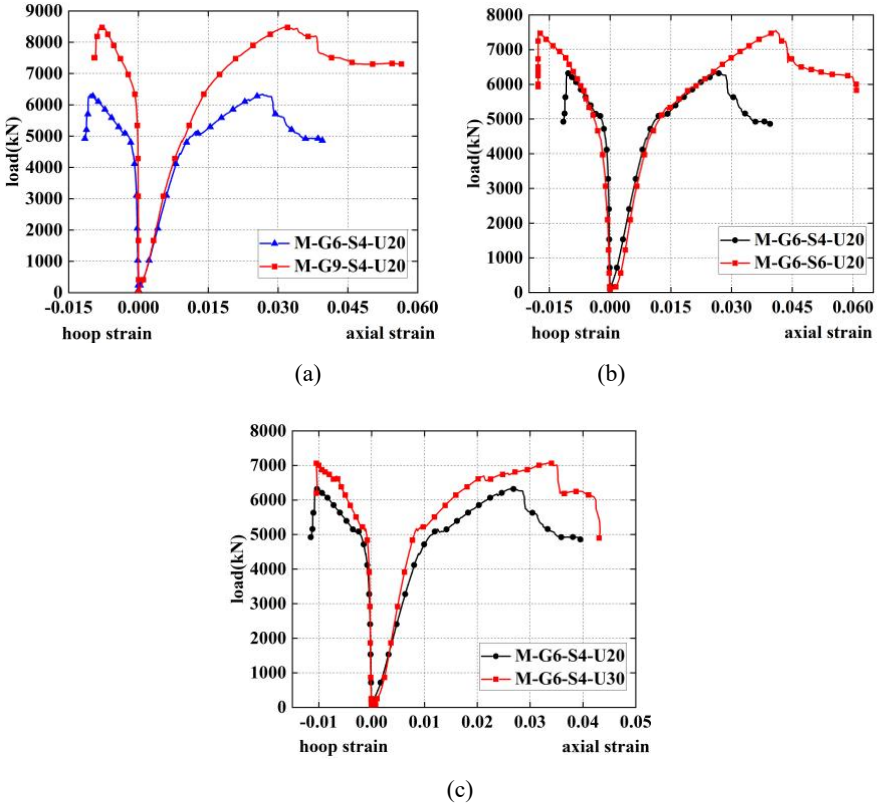


Fig. 6. Effects of different test parameters on load-strain curves: a) FRP fiber layer; b) thickness of steel tube; c) thickness of UHPC shell.

4 Conclusions

This paper conducted axial compression tests on the proposed FRP-steel-UHPC composite tube confined seawater sea-sand concrete columns (FSU-SSCs), yielding the following conclusions:

(1) Compared to traditional FRP-steel composite tubes, the addition of the UHPC shell in this FRP-steel-UHPC composite tube enhances the control over the expansion deformation of the member, particularly in effectively restricting concrete expansion, thereby improving the overall stability and integrity of the member. Furthermore, the application of the UHPC shell promotes more uniform circumferential deformation in the external steel tube.

(2) The load-displacement curve of FSU-SSCs can generally be divided into four stages: the elastic stage, the yielding stage, the development stage, and the descending stage.

(3) The synergistic effect between multiple fiber layers surpasses the performance achievable by a single layer of material, indicating that when multiple GFRP layers

work together, their mutual reinforcement effect is more than just a simple additive outcome.

(4) Increasing the number of FRP layers can effectively delay the buckling of the steel tube, extend the load development stage, and increase its slope, significantly enhancing the ultimate bearing capacity of the member. Additionally, it can withstand higher axial strain at the fracture point, exhibiting a gentler descending segment and higher residual bearing capacity. A thicker steel tube helps reduce the lateral expansion of the member, thereby enhancing the stability of the internal concrete layer and effectively delaying the initial formation and subsequent propagation of cracks in the concrete layer. A thicker UHPC shell can improve the initial stiffness and yield load of the member, extend the load development stage, and demonstrate higher ultimate bearing capacity and ultimate strain, while also restricting circumferential expansion of the concrete and improving the overall integrity of the member.

Acknowledgments

This work was financially supported by the National Natural Science Foundation of China (No. 52308252), Guangzhou Science and Technology Plan Project (No. 2025A04J2529), and Guangdong Basic and Applied Basic Research Foundation (No. 2023A1515010080), the Academician Workstation of Guizhou Province Department of Science and Technology ((2015) 4004) and the Guangzhou Municipal Science and Technology Bureau (No. 2025A03J3642).

References

1. Yasmin T, Clark J, Sambrook Smith G, Daham A, Nicholas A and Gasparotto A (2024) Towards sustainable governance of freshwater sand – A resource regime approach. *Earth Syst. Governance*, 22: 100228.
2. Wei J, Xu J, Xue J, Zhao J and Chen Z (2024) Effect of replacing freshwater river-sand with seawater sea-sand on dynamic compressive mechanical properties of concrete. *Constr. Build. Mater.*, 419: 135473.
3. Wang Q, Li L, Zhao Y, Song Y and Zhang C (2024) Feasibility assessment and application of sea sand in concrete production: A review. *Structures*, 60: 105891.
4. Nan J, Zhi C, Meng J, Miao M and Yu L (2023) Seawater aging effect on fiber-reinforced polymer composites: Mechanical properties, aging mechanism, and life prediction. *Text Res. J.*, 93: 3393–413.
5. Wu M, Xu J, Wang C, Wang P and Li W (2024) Response of columns with steel-FRP composite bars and carbon fibre reinforced polymer mesh fabric stirrups under eccentric loading. *Eng. Struct.*, 316: 118508.
6. Wang G, Wei Y, Miao K, Zheng K and Dong F (2022) Axial compressive behavior of seawater sea-sand coral aggregate concrete-filled circular FRP-steel composite tube columns. *Constr. Build. Mater.*, 315: 125737.
7. Wang Y, Chen G, Wan B, Han B and Ran J (2021) Axial compressive behavior and confinement mechanism of circular FRP-steel tubed concrete stub columns. *Compos. Struct.*, 256: 113082.

8. Lin H, Feng P and Yang J Q (2021) Pressure-dependent bond stress-slip model for sand-coated FRP-concrete interface. *Compos. Struct.*, 263: 113719.
9. Yuan C, Chen W, Pham T M, Hao H, Cui J and Shi Y (2019) Strain rate effect on interfacial bond behaviour between BFRP sheets and steel fibre reinforced concrete. *Compos. Part B-Eng.*, 174: 107032.
10. Lv L S, Wang J Y, Xiao R C, Fang M S and Tan Y (2021) Chloride ion transport properties in microcracked ultra-high performance concrete in the marine environment. *Constr. Build. Mater.*, 291: 123310.
11. Deng N, Lv G, Li W and Chen Z (2024) Study of the UHPC-NC interfacial bonding properties of steel tubes with internally welded reinforcement rings. *Appl Sci-Basel* 2024; 14: 5604.
12. Dong Z, Wu G, Zhao X L, Zhu H and Shao X (2019) Behaviors of hybrid beams composed of seawater sea-sand concrete (SWSSC) and a prefabricated UHPC shell reinforced with FRP bars. *Constr. Build. Mater.*, 213: 32–42.
13. Liu D, Wu Z, Lin L, Wu X, Zhang Y and Wu C (2024) Behaviors Analysis of High Performance Composite Bearing Cap Made by UHPC Permanent Form for Offshore Wind Tower Foundation. *Proceedings of ICCEA 2023*, 85–92.

Open Access This chapter is licensed under the terms of the Creative Commons Attribution-NonCommercial 4.0 International License (<http://creativecommons.org/licenses/by-nc/4.0/>), which permits any noncommercial use, sharing, adaptation, distribution and reproduction in any medium or format, as long as you give appropriate credit to the original author(s) and the source, provide a link to the Creative Commons license and indicate if changes were made.

The images or other third party material in this chapter are included in the chapter's Creative Commons license, unless indicated otherwise in a credit line to the material. If material is not included in the chapter's Creative Commons license and your intended use is not permitted by statutory regulation or exceeds the permitted use, you will need to obtain permission directly from the copyright holder.

